

Article

Heat-Transfer Characteristics of Liquid Sodium in a Solar Receiver Tube with a Nonuniform Heat Flux

Jing Liu ¹, Yongqing He ^{1,*}  and Xianliang Lei ²

¹ School of Chemical Engineering, Kunming University of Science and Technology, Kunming 650500, China; Jedxy1037@gmail.com

² State Key Laboratory of Multiphase Flow in Power Engineering, Xi'an Jiaotong University, Xi'an 710049, China; xianlianglei@xjtu.edu.cn

* Correspondence: yqhe@kmust.edu.cn

Received: 7 March 2019; Accepted: 11 April 2019; Published: 14 April 2019



Abstract: This paper presents a numerical simulation on the heat transfer of liquid sodium in a solar receiver tube, as the liquid sodium is a promising heat-transfer candidate for the next generation solar-power-tower (SPT) system. A comparison between three mediums—solar salt, Hitec and liquid sodium—is presented under uniform and nonuniform heat-flux configurations. We studied the effects of mass flow rate (Q_m), inlet temperature (T_{in}), and maximum heat flux ($q_{o,max}$), on the average heat-transfer coefficient (h) and the friction coefficient (f) of the three mediums. The results show that the h of liquid sodium is about 2.5 to 5 times than other two molten salts when T_{in} is varying from 550 to 800 K, Q_m is 1.0 kg/s, and $q_{o,max}$ is 0.1 MW/m². For maximum heat fluxes from 0.1 to 0.3 MW/m², the h of liquid sodium is always an order of magnitude larger than that of Hitec and Solar-Salt (S-S), while maintaining a small friction coefficient.

Keywords: solar-power tower; liquid sodium; solar salt; Hitec; heat flux

1. Introduction

Compared to the parabolic trough, Fresnel and dish collectors, the solar-power-tower (SPT) plant has the remarkable advantages, such as lower electricity cost, large-scale power generation and higher efficient thermodynamic cycles [1–3]. The SPT is equipped with a large number of heliostats on the ground, each with a tracking mechanism that accurately reflects the reflection of sunlight onto the receiver at the top of a tall tower. The concentrating magnification on the receiver can exceed 1000 times. One typical arrangement of the SPT receivers is the external tubular receiver designed for Solar Two project, in which only half of the surface of the tube is exposed to solar irradiation. This may bring about many problems, such as aggravating the plastic deformation of the receiver tube, facilitating degradation of the selective absorptive coating and decreasing the allowable solar heat flux [4,5]. Since the nonuniform solar heat flux tends to cause the temperature inhomogeneity of the heat-transfer fluid (HTF) and, further, the thermal stress on the heat-transfer tubes, a much broader range of operational temperatures is required. The liquid metal as the promising candidate for the exposed cylindrical heat absorber of SPT has been proposed [6].

Nitrate salts have been used as HTFs and thermal storage mediums for decades in the concentrating SPT industry. The most commonly used HTFs are solar salt (S-S, 60% NaNO₃ and 40% KNO₃) and Hitec (53% KNO₃ + 40% NaNO₂ + 7% NaNO₃). Both the nitrate salt mixtures will decompose above 873 °K, which has seriously limited the overall efficiency in the SPT system. Furthermore, recent research efforts have shown that the nitrate salts are more suitable for use in parabolic trough systems due to their low working temperature [7]. However, the next-generation SPT systems require a higher incident peak flux and operating temperature. If the liquid metal is the heat-transfer fluid, it can

provide an incident peak flux above 0.6 MW/m^2 . Liquid sodium (Na), characterized by chemical stability at temperatures up to near $1173 \text{ }^\circ\text{K}$ has a lower melting point to $371 \text{ }^\circ\text{K}$ [8], as well as superior thermal conductivity and low Prandtl number. The material properties mentioned above can largely improve heat transfer when compared to conventional fluids such as oil or salt mixtures [9]. In fact, during the early years of the development of central receiver systems (CRSs), liquid sodium was one of the prominent HTFs under investigation. Indeed, several test projects have been developed, and the efficiency was obtained at 88%–96% in the 1980s [10]. However, the disadvantage of liquid sodium is its high combustibility when in contact with water even if no air. Fortunately, special and protective measures have also been developed from previous experiences [11]. Also, this technology has continued to be investigated by several institutions around the world [12–14]. Besides, further work has reported that liquid metals have attractive properties for CSP applications [15,16]. Recently, Amy et al. [17] demonstrated how a ceramic, mechanical pump that can be used to continuously circulate liquid metal at temperatures of around $1473 \text{ }^\circ\text{K}$ – $1746 \text{ }^\circ\text{K}$. This study solves the problem that collecting, transporting, storing liquid metal above $1300 \text{ }^\circ\text{K}$ brings.

The prediction of heat transfer of liquid metal has been the subject of many investigations. DeAngelis et al. [18] have examined using a liquid metal as heat-transfer fluid in conjunction with a receiver. It is feasible to reach temperatures of $1623 \text{ }^\circ\text{K}$ at greater than 90% efficiency. Boerema et al. [15] compared liquid sodium and Hitec, and the use of liquid sodium can achieve 57% absorber area reduction and 1.1% efficiency improvement. Even if liquid sodium is an excellent heat-transfer medium, the specific application background was not mentioned in the paper. Pacio et al. [19,20] summarized the current state-of-the-art of liquid metals (LMs) as HTFs in solar power plants.

Additionally, the liquid sodium (Na) was proposed as an efficient HTF to allow extending the design ranges, and able to contribute to the development of next-generation SPT. Matsubara et al. [21] studied the spanwise heat transport in turbulent channel flow with Prandtl numbers ranging from 0.025 to 5.0. It is regrettable that they do not compare the heat-transfer property with traditional heat-transfer fluid (e.g., solar salts). Rodríguez-Sánchez et al. [22,23] focused on the thermal, mechanical and hydrodynamic analysis associated to the nonuniformity of the heat flux, and they also considered the thermal field and thermal stresses along the solid wall [24].

A higher cost, more complex system and security issues are factors that have to be considered for the experimental research on liquid metal.

Therefore, numerical simulation is an effective research method [25,26]. In this work, we present a numerical simulation on the heat transfer of liquid sodium under nonuniform heat flux. A physical model of a single tube is established to investigate the heat-transfer performance of the receiver tube, and two other commonly used heat-transfer media, Hitec and solar salt, are also to be considered. First, we built solar heat-flux distributions on the whole absorber outer wall and circumferential variation of heat flux on the inner wall of the tube. Then, the heterogeneity of the temperature on the circumferential tangent plane and the solid wall is presented. Cloud images show the wall temperature distribution of the three HTFs. The temperature difference ($\Theta - \Theta_{\text{ref}}$) of the three HTFs along the circumferential angle is compared when q_{omax} is 0.1 MW/m^2 , Re is ranging from 10,000 to 30,000, and inlet temperature is $550 \text{ }^\circ\text{K}$. Last, the influence of three parameters, Q_m (1.0 to 3.0 kg/s), q_{omax} (0.1 to 0.3 MW/m^2), T_{in} ($550 \text{ }^\circ\text{K}$ to $800 \text{ }^\circ\text{K}$) on the heat-transfer characteristics of sodium, S-S and Hitec are discussed. This research can offer technical references for the design and construction of experimental facilities.

2. Mathematical model

2.1. Physical Model

The research background of this study is the heat receiver of the solar-power-tower system (Figure 1a). Since the collector is cylindrical and the fluid flows serpentine in the collector tube, we investigate only the single collector tube (Figure 1b).

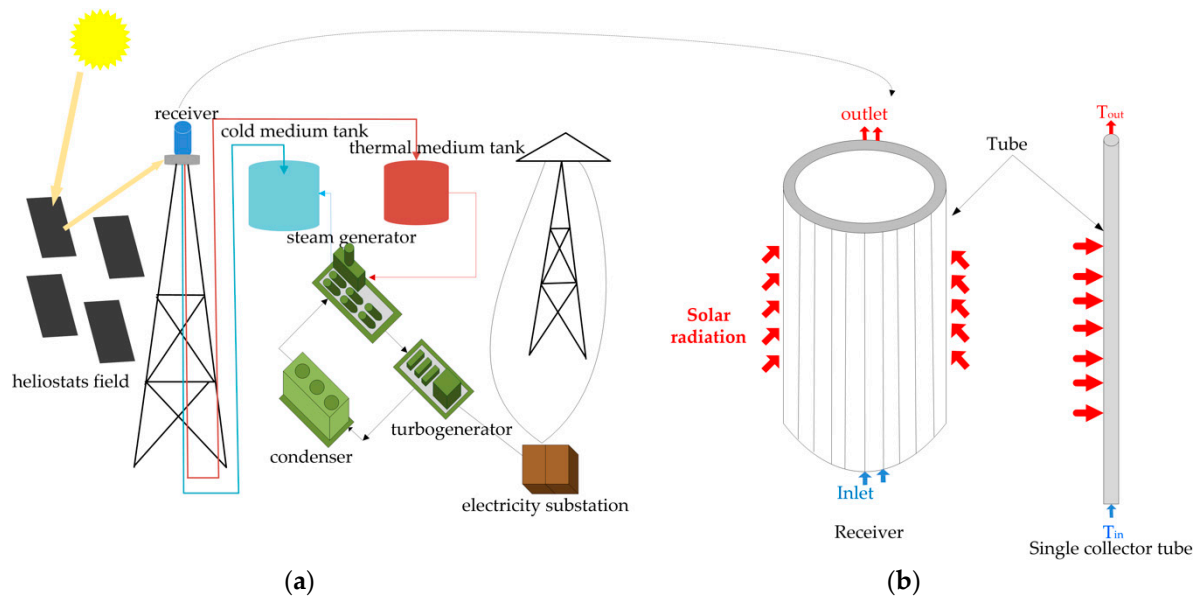


Figure 1. (a) Solar power tower system; (b) Exposed cylindrical heat receiver and a single receiver tube

We consider the conjugate heat-transfer problem of a receiver tube subject to inhomogeneous heat flux along the axial direction (z), circumferential direction (θ), and radial direction (r). The heat transport from the regional source (see Figure 2) contains three orthogonal components. The outer diameter (R) of the geometric model is 20 mm, and the tube length is $100R$. The effect of different thermal boundary conditions on the heat-transfer performance of the collector tube is discussed.

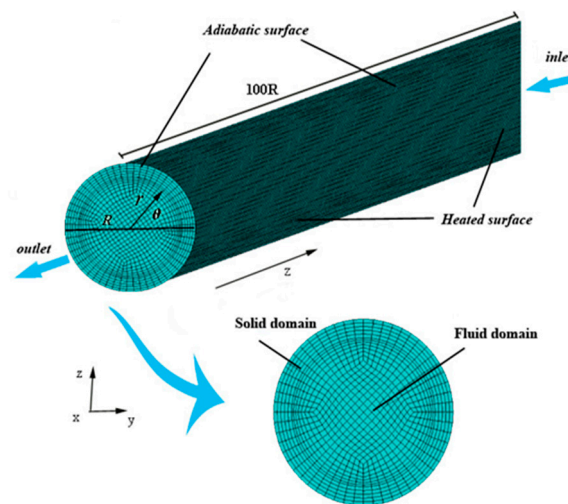


Figure 2. Schematic diagram of tower solar collector.

As shown in Figure 3, this paper deals with two heat-flux conditions of the turbulent-flow model: (a) A cosine heat flux (see Equation (1)) [27] is imposed on one half of the wall of the tube, while the other half is considered adiabatic.

$$q = \begin{cases} q_{o\max} \cdot e^{-\frac{9}{2} \cdot (z-1)^2} \cdot \cos \theta, & \cos \theta \geq 0 \\ 0, & \cos \theta < 0 \end{cases} \quad (1)$$

where the $q_{o\max}$ is the maximum heat flux on the wall of the collector tube, θ is the circumferential angle, and z is the length along the axial direction of the receiver tube.

(b) The heat flux to the bright side is constant, and the backlight side is an adiabatic.

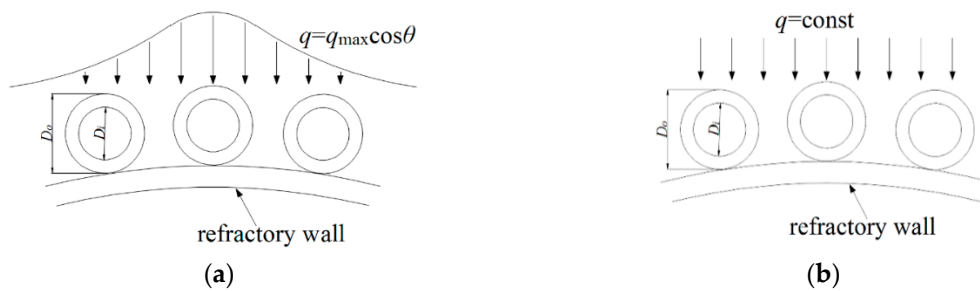


Figure 3. The heat flux conditions: (a) nonuniform heat flux (NHF) (b) uniform heat flux (UHF).

2.2. Governing Equations

A conjugate heat-transfer model is adopted to obtain the heat flux and temperature distribution in both the fluid and the tube wall. To simplify the model, the following assumptions are made: (1) the mediums are homogeneous and isotropic; (2) the liquid phase is in a state of local thermal equilibrium; (3) the heat loss at the outer wall of the receiver tube is not considered since this paper only focuses on the heat-transfer characteristic of the HTFs in the tube. For the heat loss on the outer surface of the tube, one can refer to the references [23,28].

The governing equations for continuity, momentum, energy and standard k - ε two-equation turbulence model for the incompressible Newtonian fluid can be expressed as follows:

Continuity equation:

$$\frac{\partial}{\partial x}(\rho u_i) = 0, \quad (2)$$

Momentum equation:

$$\frac{\partial}{\partial x_i}(\rho u_i u_j) = -\frac{\partial p}{\partial x_i} + \frac{\partial}{\partial x_j}[(\mu_t + \mu) + (\frac{\partial u_i}{\partial x_j} + \frac{\partial u_j}{\partial x_i}) - \frac{2}{3}(\mu_t + \mu)\frac{\partial u_l}{\partial x_l}\delta_{ij}] + \rho g_i, \quad (3)$$

Energy equation:

$$\frac{\partial}{\partial x_i}(\rho u_i T) = \frac{\partial}{\partial x_i}[(\frac{\mu}{Pr} + \frac{\mu_t}{\sigma_t})\frac{\partial T}{\partial x_i}] + S_R, \quad (4)$$

k equation:

$$\frac{\partial}{\partial x_i}(\rho u_i k) = \frac{\partial}{\partial x_i}[(\mu + \frac{\mu_t}{\sigma_k})\frac{\partial k}{\partial x_i}] + G_k - \rho \varepsilon, \quad (5)$$

ε equation:

$$\frac{\partial}{\partial x_i}(\rho u_i \varepsilon) = \frac{\partial}{\partial x_i}[(\mu + \frac{\mu_t}{\sigma_\varepsilon})\frac{\partial \varepsilon}{\partial x_i}] + \frac{\varepsilon}{k}(c_1 G_k - c_2 \rho \varepsilon), \quad (6)$$

where the turbulent viscosity μ_t and the production rate of k G_k are given by

$$\mu_t = c_\mu \rho \frac{k^2}{\varepsilon}, \quad G_k = \mu_t (\frac{\partial u_i}{\partial x_j} + \frac{\partial u_j}{\partial x_i}), \quad (7)$$

where the standard constants are employed, $c_\mu = 0.09$, $c_1 = 1.44$, $c_2 = 1.92$, $\sigma_k = 1.0$, $\sigma_\varepsilon = 1.3$, and $\sigma_T = 0.85$ [29].

2.3. Boundary Conditions

As a plurality of solar mirrors superposes the heat flux to the receiver tube wall, the radiation heat flux is highly nonuniform. The heat-flux expression is approximating the normal distribution function along the axial direction of the receiver tube and the cosine function distribution along the circumferential direction, as described in the Formula (1).

It is also convenient to define the total heat flux applied to the outer surface, and note that the energy conservation in the solid implies that:

$$Q = \int_0^\pi q_0(\theta)R_0d\theta = 2q_{0max}R_0, \quad (8)$$

where the total heat flux (Q) is kept constant for all the cases presented here, and $R_0 = 20$ mm.

Considering the wall temperature of the tube varies with the time and heat flux, to improve the accuracy and practicability of the numerical calculation, we adopted the formulas shown in Table 1 to evaluate the thermophysical properties of HTFs. The collector tube material is 316 L stainless steel, and its thermal conductivity (k_s) is 18.4 W/(m·K). Based on the assumptions, the boundary conditions are expressed as follows:

Table 1. Thermophysical properties of sodium [30], Solar salt and Hitec [7], where T is the fluid bulk temperature in Kelvin.

HTFs	Thermophysical Properties	Property Equation
Liquid sodium 371 °K–1255 °K	$\rho/\text{kg}\cdot\text{m}^{-3}$	$219 + 275.32(1 - T/2503.7) + 511.58(1 - T/2503.7)^{0.5}$
	$\lambda/\text{W}\cdot\text{m}^{-1}\cdot\text{K}^{-1}$	$124.67 - 0.11381\cdot T + 5.5226 \times 10^{-5}\cdot T^2 - 1.1842 \times 10^{-8}\cdot T^3$
	$c_p/\text{J}\cdot\text{kg}^{-1}\cdot\text{K}^{-1}$	$1658.2 - 0.84790\cdot T + 4.4541 \times 10^{-4}\cdot T^2 - 2.9926 \times 10^6\cdot T^{-2}$
	$\mu/\text{Pa}\cdot\text{s}$	$\ln(T) = -6.4406 - 0.3958\ln(T) + 556.835/T$
Solar salt 533 °K–873 °K	$\rho/\text{kg}\cdot\text{m}^{-3}$	$2090 - 0.636(T - 273.15)$
	$\lambda/\text{W}\cdot\text{m}^{-1}\cdot\text{K}^{-1}$	$0.443 + 1.9 \times 10^{-4}(T - 273.15)$
	$c_p/\text{J}\cdot\text{kg}^{-1}\cdot\text{K}^{-1}$	$1443 + 0.172(T - 273.15)$
	$\mu/\text{Pa}\cdot\text{s}$	$2.2714 \times 10^{-2} - 1.2 \times 10^{-4}(T - 273.15) + 2.281 \times 10^{-7}(T - 273.15)^2 - 1.474 \times 10^{-10}(T - 273.15)^3$
Hitec 415 °K–808 °K	$\rho/\text{kg}\cdot\text{m}^{-3}$	$-0.74(T - 273.15) + 2084$
	$\lambda/\text{W}\cdot\text{m}^{-1}\cdot\text{K}^{-1}$	$0.411 + 4.36 \times 10^{-4}(T - 273.15) + 1.54 \times 10^{-6}(T - 273.15)^2$
	$c_p/\text{J}\cdot\text{kg}^{-1}\cdot\text{K}^{-1}$	$1560 - (T - 273.15)$
	$\mu/\text{Pa}\cdot\text{s}$	$10^{2.7374}(T - 273.15)^{-2.104}$

(1) Fluid and the solid wall region

When the HTF flows around a stationary solid wall in a collector tube, where the solid wall is impermeable, the normal velocity should be satisfied $v_n = 0$. At the same time, the no-slip condition must be satisfied, and the tangential velocity $v_\tau = 0$. The heat-flux condition of the tube wall is:

$$q_w = -(\lambda \frac{\partial T}{\partial n}), \quad (9)$$

(2) The inlet and outlet temperature of the tube

The inlet velocity, pressure, and temperature of the tube line are formulated as follows, respectively.

$$T_{x=0} = T_0, u_{x=0} = u_0, p_{\text{inlet}} = p_0. \quad (10)$$

2.4. Numerical Methods

The governing Equations (2)–(7) are discretized by the finite volume method by using O-mesh and wall-dense nonuniform mesh. Moreover, the convective terms in momentum and energy equations are discretized with the second upwind scheme. The SIMPLE algorithm is used to ensure the coupling between velocity and pressure. The discretization of momentum, turbulent kinetic energy, energy, and dissipation rate are all second upwind schemes. The turbulence model is κ - ϵ model. The near-wall surface flow is solved by the standard wall function method, and all the non-dimensional number of near-wall y^+ is controlled by 30~60. The convergence criterion for the velocities and energy is that the

maximum mass residual of the cells divided by the maximum residual is less than 10^{-5} and 10^{-7} for the continuity, momentum, and energy equation. Based on these methods, the performance of the receiver tube for the two models with different HTFs can be rapidly predicted [31].

2.5. Parameter Definitions

To predict the thermal and hydraulic characteristics, we define the time-averaged temperature in the cross-plane among the fluid as Θ , and the average temperature of the inlet and outlet of a receiver tube is named Θ_{ref} , also known as the qualitative temperature.

The Reynolds number and average Nusselt number in the receiver tube for the medium are given as [32].

$$Re = \frac{uD_i\rho}{\mu}, Nu = \frac{hR_i}{\lambda}, h = \frac{q}{\Delta t}, \quad (11)$$

where h is the average heat-transfer coefficient, q is the average heat flux in the tube, Δt the difference between the average temperature of the inner wall of the tube and the qualitative temperature.

The friction coefficient is defined as [33]:

$$f = \frac{\Delta p}{L} \frac{R_i}{(1/2)\rho u^2}, \quad (12)$$

where Δp is the pressure difference between the inlet and outlet of the receiver tube.

3. Model Verification and Cases Studied

3.1. Model Verification

We verified the calculation procedure by comparing them with empirical formulas and existing experimental data. Figure 4a exhibits the trend of Nu for S-S ($Pr = 13$) and Hitec ($Pr = 50$) as the Re ranging from 1×10^4 to 3×10^4 under the nonuniform heat flux on a receiver tube. The inlet temperature is set as the melting point for the three HTF, respectively. The result of the calculation is in good agreement with Dittus–Boetter correlation and Gnielinski correlation [7]. Figure 4b shows the variation tendency of Nu when the Pe is ranging from 65 to 203 for sodium ($Pr = 0.01$). The calculation results have a 2~6% difference with the Lyon–Martinelli equation correlation [34] and are consistent with the experimental data [30]. These results prove that the model and its calculation procedure is suitable and reasonable.

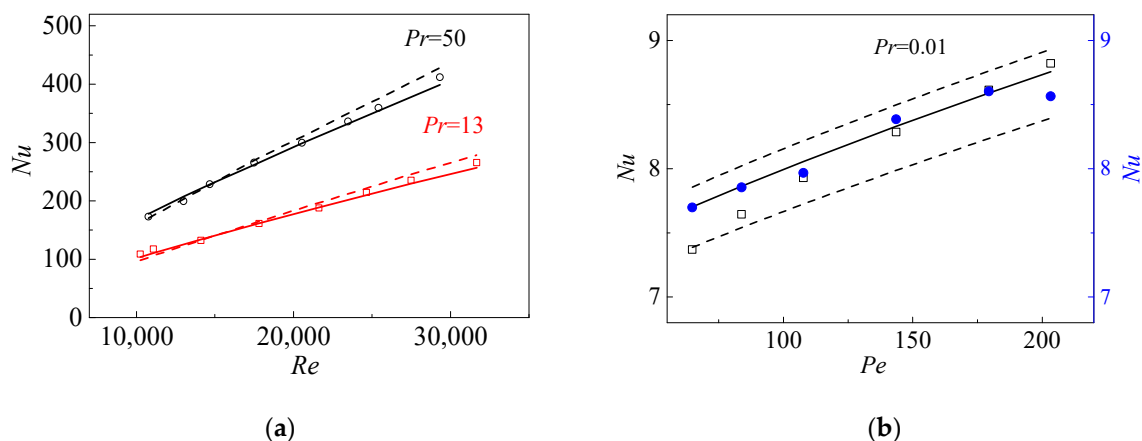


Figure 4. (a) Nu , as a function of Re , computed with inhomogeneous heating with $WTR = 0.125$. Red squares: $Pr = 13$. Black circles: $Pr = 50$. Solid lines: Dittus–Boetter correlation. Dashed lines: Gnielinski correlation. (b) Nu , as a function of the Péclet number, Pe . Solid lines: Lyon–Martinelli correlation ($Nu = 7 + 0.028 \cdot Pe^{0.8}$). Dashed lines refer to 2~6% from the correlation. Blue points: experimental data [34]. Black squares: numerical results.

3.2. Cases Studied

The main parameters used in the calculation cases are listed in Table 2. Among them, the mass flow rate varies from 1.0 to 3.0 kg/s, $q_{o\max}$ is from 0.1 to 0.3 MW/m², and the inlet temperature is from 550 °K to 800 °K. The temperature range is chosen between the melting point and the boiling point of the three mediums.

Table 2. The calculation parameters.

Test Condition	HTFs	Q_m (kg/s)	T_{in} (°K)	$q_{o\max}$ (MW/m ²)	h (W/m ² K)
Case1	Sodium	1.0~3.0	550	0.1	2989~14,089
	S-S				2105~7318
	Hitec				2526~7947
Case2	Sodium	1.0	550~800	0.1	23,822~21,520
	S-S				4859~10,107
	Hitec				6047~11,664
Case3	Sodium	1.0	550	0.1~0.3	75,960~75,753
	S-S				5502~5581
	Hitec				6047~6167

4. Results and Discussion

4.1. Heat Flux

The heat-flux distributions on the whole absorber outer wall (case 1) are consistent with the result of Equation (1) shown in Figure 5.

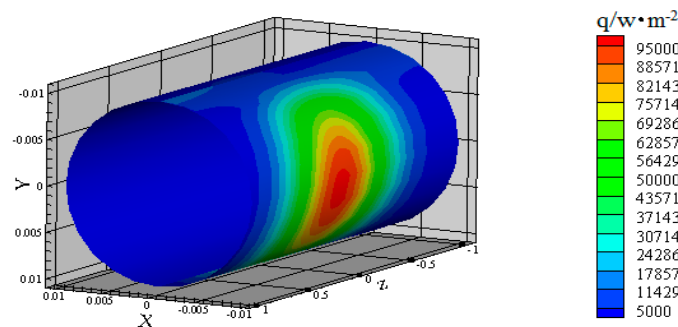


Figure 5. 3D heat-flux distribution on the outer tube's wall.

Figure 6 shows that the solar energy flux distribution, of different mediums on a cross section when Q_m is set as 1 kg/s, the inlet temperature is 550 °K, and $q_{o\max}$ is 0.1 MW/m². The distribution is unsymmetrical in the circumferential direction and is independent of the HTF in the receiver tube. It is noteworthy that the maximum heat flux through the inner wall is at the location 90°.

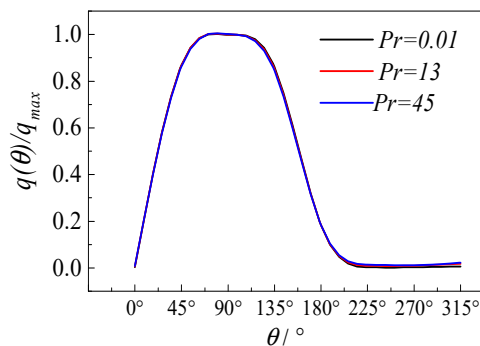


Figure 6. Circumferential variation of heat flux on the inner wall of the tube. The heat flux is non-dimensional with the maximum heat flux $q_{o\max}$ at the same WTR and Re .

4.2. Temperature Profile

The heat-flux distribution caused by inhomogeneous radiation inevitably influences the temperature distribution on the collector tube. The heterogeneity of the temperature on the circumferential tangent plane and the solid wall is shown in Figures 7 and 8. The coupled heat transfer between solid wall and fluid has been omitted in this section.

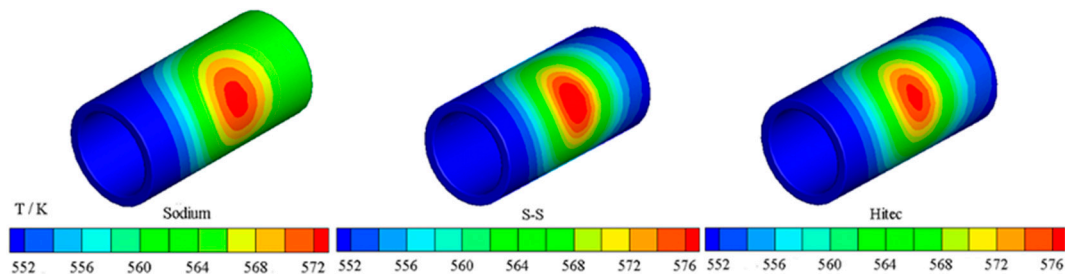
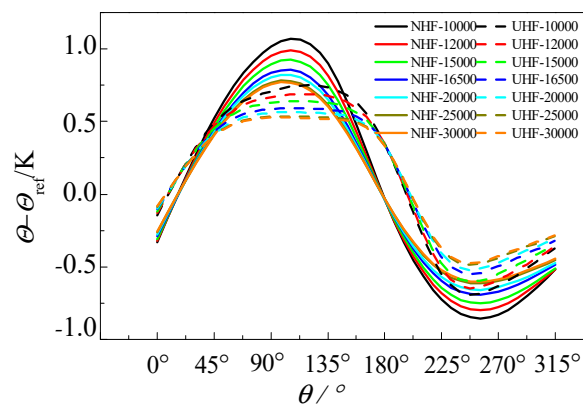


Figure 7. Temperature distribution on tube wall of sodium, S-S, and Hitec.

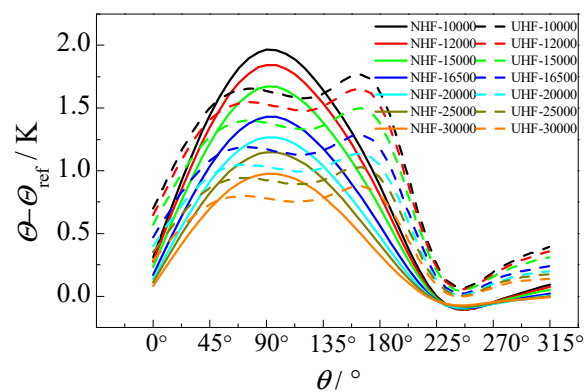
When the Re is 25,000, and the inlet temperature is 550 °K, the wall temperature distributions of the three HTFs are shown in Figure 7. It is found that the temperature distribution on the outer wall is extremely nonuniform around the tube. Compared with the other two HTFs, the temperature distribution on the solid wall of sodium is more uniform at the exit section. The outlet temperature is 561.08 °K, 550.93 °K, 551.06 °K on the area-weight-average from left to right of Figure 7. The tube wall temperature difference of sodium changes to 20 °K, solar salt changes to 24 °K and the Hitec changes to 24 °K after passing through two meters of the tube. Overall, for sodium, the temperature difference of the whole tube is the minimal, and the outlet temperature is higher than S-S or Hitec. The reasons for those are that high thermal conductivity of sodium, which enhances the turbulent flow, the heat transfer and reduces the wall temperature. Thus, in SPT projects, sodium is more suitable as a heat-transfer medium than S-S or Hitec, in terms of flow dynamics and heat transfer.

Figure 8 shows the variation of the temperature difference as a function of the circumferential coordinate. We made a comparison between the present NHF model calculations (solid-lines) and the results predicted by the uniform heat flux (UHF) model (dashed lines). The temperature difference ($\Theta - \Theta_{ref}$) means the difference in the temperature on the circumferential section and the qualitative temperature. The temperature difference ($\Theta - \Theta_{ref}$) of the three HTFs along the circumferential angle is compared when $q_{o,max}$ is 0.1 MW/m², Re is ranging from 10,000 to 30,000, and inlet temperature is set to 550 °K.

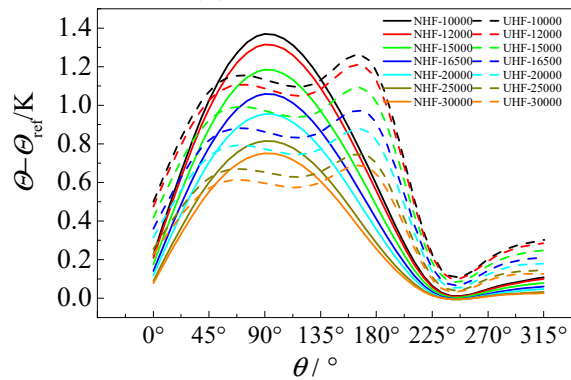
Note that the UHF model underestimates the inner temperature of the tube on the bright side while overestimates the backlight since the UHF model imposed the same heat flux on the bright side. Energy accumulation on both sides of the tube leads to two highest temperature points shown in Figure 8b,c whereas sodium has no obvious highest point. In the UHF model, the $\Theta - \Theta_{ref}$ of sodium is lower than that in the NHF model, and the temperature difference is considerable as Re increasing. The results indicate that thermal conductivity still dominates even if the turbulence is significant when sodium is used as HTF. For the higher Prandtl number (S-S or Hitec), the average temperature in cross-plane of the adiabatic side must be equal to the bulk temperature. The reason is that the momentum transfer rate is higher than the heat-transfer rate, so the velocity surface is first established, and the heat-transfer delay. The changing range of $\Theta - \Theta_{ref}$ is larger than sodium as Re increasing for S-S or Hitec. That shows that the flow and heat transfer of S-S or Hitec are greatly influenced by turbulence. As expected, the maximum temperature difference reached at the location of 90°, which agrees with the cosine effect expressed by the Equation (1).



(a) Liquid sodium



(b) Solar salt



(c) Hitec

Figure 8. (a–c) Circumferential variation of the inner wall fluid temperature with the qualitative temperature for different Reynolds number at a fixed-inlet temperature ($T_{in} = 550$ °K). (a) $Pr = 0.001$ (b) $Pr = 13$ (c) $Pr = 50$. Solid lines: the present calculations; Dashed lines: homogeneous heat-flux model (HHFM).

The value of $\Theta - \Theta_{ref}$ is slightly dependent on the Re but strongly affected by the Pr . In general, the $\Theta - \Theta_{ref}$ is increasing as the Pr increases, decreasing as the Re increases. Comparing Figure 8a–c, the temperature difference of S-S at the location $\theta = 90^\circ$ is 1.93 times higher than sodium, and Hitec is 1.35 times higher that of sodium when Re is 10,000. The temperature difference of S-S is 1.29 times higher than sodium, and Hitec is 2.0 times sodium when Re is 30,000. The results reflect that sodium has a good effect on solving the uneven temperature caused by nonuniform heat flux, which may reduce the risk of hot spots and, thus, reduce pipe stresses.

Another concern is the inner wall temperature, also called film temperature, which could lead to the degradation of the HTFs. The inner wall temperature distribution in NHF and UHF models are shown in Figure 9a–c when Re is 25,000, and the inlet temperature is 550 K. From Figure 9a–c, the average temperature of the fluid in the tube is: 562.8 °K, 554.9 °K, 554.7 °K. Figure 9a–c show that one of the most significant advantages of sodium over S-S and Hitec is that the temperature distribution is much more uniform on both the inner and outer surface of the tube.

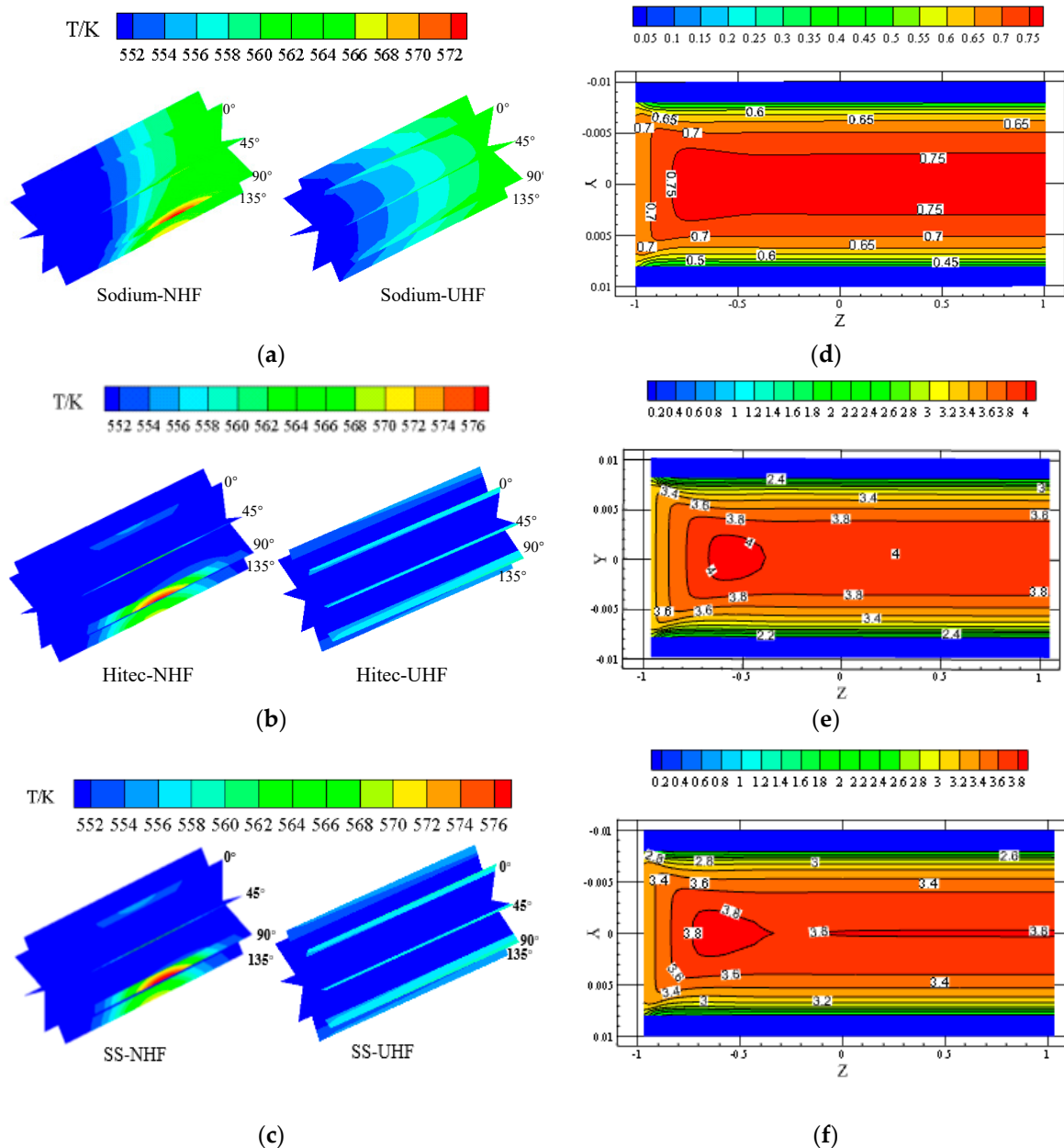


Figure 9. (a–c) Temperature distribution of three kinds of media under two models and (d,e) velocity distribution under NHF model.

Obviously, for the NHF model, there is a heat spot on the outer wall from 0° to 180°, especially at 90°. At the same time, the UHF model is idealistic. But, the highest heat spot temperature of sodium is the lowest, while S-S and Hitec are same. There is a considerable temperature gradient when the sodium flows in the receiver tube. Besides, not far from the entrance, the inner fluid temperature is higher and more uniform than S-S or Hitec flow in the tube.

Corresponding velocity distribution is shown in Figure 9e,f. The velocity of sodium is the lowest, only 0.19 times the other two mediums. At a distance of 0.2 m from the inlet, the sodium flow reached fully developed, and the boundary layer is thinner, while the other boundary conditions remained unchanged. It can be explained that the molecule heat conduction of sodium dominates in fully developed turbulent heat transfer. The heat diffusion of the medium with lower Prandtl number (sodium) is much higher than the momentum transfer diffusivity.

4.3. Effects of Mass Flow

Figure 10 shows the dependence of h, f of the three HTFs on Q_m , which varies from 0.2 to 1.4 kg/s. The values of maximum heat flux and inlet temperature are set to 0.1 MW/m^2 and $550 \text{ }^\circ\text{K}$, respectively.

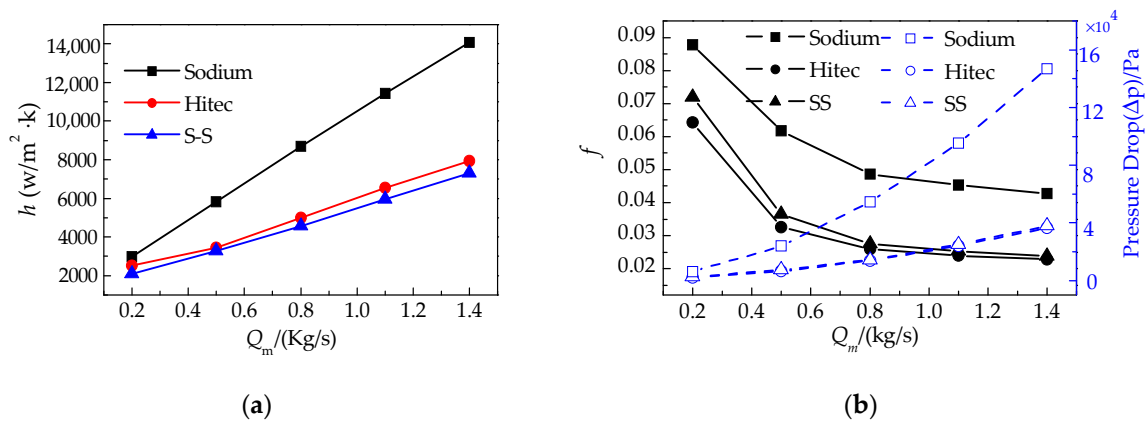


Figure 10. Effects of Q_m on the heat-transfer performance of the HTFs in the tube: (a) Q_m - h , (b) Q_m - f - Δp .

The average heat-transfer coefficient of all working fluids increases with the mass flow. When the Q_m increases by 0.3 kg/s , the h of S-S, Hitec and sodium increases by an average of 1303, 1355, $2775 \text{ W/m}^2 \cdot \text{K}$, respectively. The variation of Q_m has a significant influence on the heat-transfer characteristic of the HTFs, especially on sodium. For sodium, the higher the Q_m , the better the heat-transfer coefficient. The reason is that the average temperature difference is getting smaller increasingly with the rise of Q_m when the maximum heat flux is 0.1 MW/m^2 . However, the law of change in the average friction coefficient is reversed, all decreasing as the flow rate increases. When the Q_m is higher than 0.8 kg/s , the friction coefficient decreases slowly. S-S and Hitec, with high heat-transfer rate and low-pressure drop, are exceptionally beneficial for heat transfer. The results suggest that the Q_m should be higher than 0.8 kg/s to obtain greater heat-transfer performance. However, a larger mass-flow rate represents more considerable pump pressure and more substantial heat absorption capability. Besides, without increasing the solar thermal input, it is possible to cause the reduction of fluid temperature and increase the corresponding heat loss.

4.4. Effects of Inlet Temperature

The physical properties of the HTF are primarily affected by the inlet temperature (T_{in}). The typical operating temperatures for the three HTFs are shown in Table 3. The available temperature range is between the melting point and the boiling point. The trends of h, f for the three HTFs have been shown in Figure 11. T_{in} is varying from $550 \text{ }^\circ\text{K}$ to $800 \text{ }^\circ\text{K}$, Q_m is 1.0 kg/s , and $q_{o\text{max}}$ is 0.1 MW/m^2 .

From Figure 11a, the heat-transfer coefficient of sodium is larger by about 2.5 to 5 times than the other two kinds of molten salt and decreases slowly with the temperature rising. The reason for the above unique heat-transfer feature of sodium is its high conductivity, and it decreases with increasing temperature even in turbulent flow. As shown in Figure 11c, the conductivity of sodium is 118, 154 times Hitec and S-S at $550 \text{ }^\circ\text{K}$, respectively. Furthermore, the h of Hitec or S-S increases linearly with the increase of temperature whereas sodium is the opposite. The h of Hitec has not changed significantly

between 750 °K and 800 °K because its boiling point is 808 °K. The greater the h , the smaller the f when the mass-flow rate is constant for the three HTFs. Besides, from Table 3, the energy-storage capacity (ρC_p) of Hitec or S-S is two times more than the sodium.

Table 3. Comparison of the physical properties for different HTFs proposed for CRS applications. The physical properties are evaluated at 550 °K, 1 bar. melting point = m.p, normal boiling point (n.b.p). Sources: [35–37].

Candidate HTF	m.p °K	n.b.p °K	ρC_p kJ/m ³ .°K
Sodium	371	1255	1166
Solar salt	533	873	2498
Hitec	415	808	2411

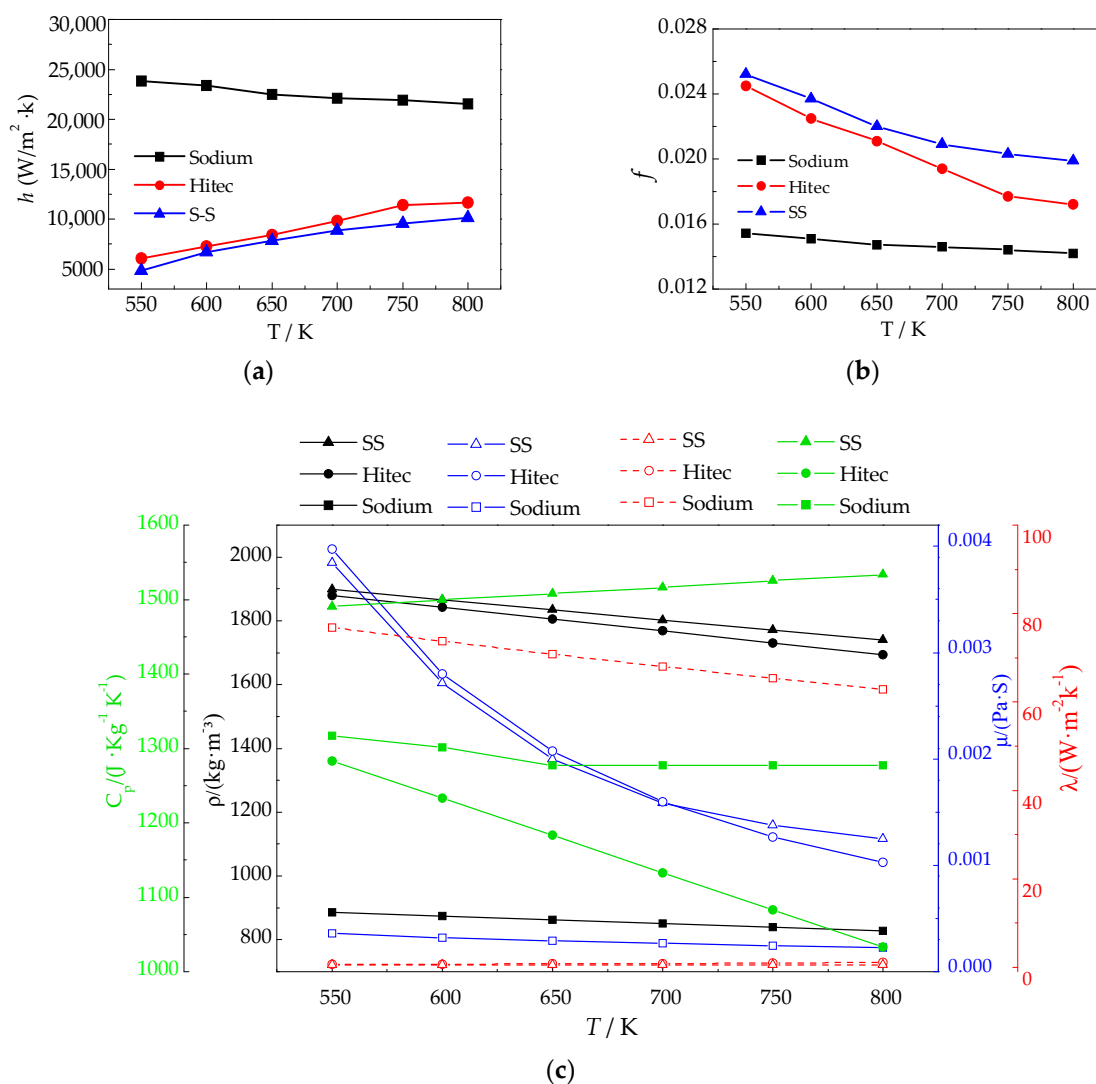


Figure 11. Effects of T_{in} on the performance of tube: (a) T - h ; (b) T - f ; (c) T - ρ - μ - C_p - λ .

Based on the above conclusions, we can select sodium as the heat-transfer medium in the collector tube on the top of the SPT, while the Hitec or S-S as the circulating medium or storage medium, respectively.

4.5. Effects of Heat Flux on the Outside Surface

Generally, the heat flux on the outside surfaces of the receiver tubes in SPT plants is quite limited to give a reasonable lifetime. The maximum heat flux allowed (allowable flux density), q_{0max} , has progressively grown for many years, such as 0.35 MW/m² in the Solar One plant and 0.8 MW/m² in the Solar Two plant. Besides, the q_{0max} is a crucial parameter for the receiver design, since it is directly related to the heliostat field cost, which involves the number of heliostats and the arrangement strategy [38,39].

Figure 12a,b show the variations of h, f of the three HTFs when q_{0max} varies from 0.1 to 0.3 MW/m². The values of mass flow rate and inlet temperature are set to 1.0 kg/s and 550 °K, respectively. The increased maximum heat flux does not affect the average heat-transfer coefficient of HTFs in the tube, and the h of sodium is invariably 12.56 times that of Hitec and 13.8 times that of S-S. At the same time, the flow of liquid sodium in the tube maintains a small friction coefficient compared to the other two working fluids (Figure 12b). Therefore, liquid sodium ensures economics while maintaining efficient system operation.

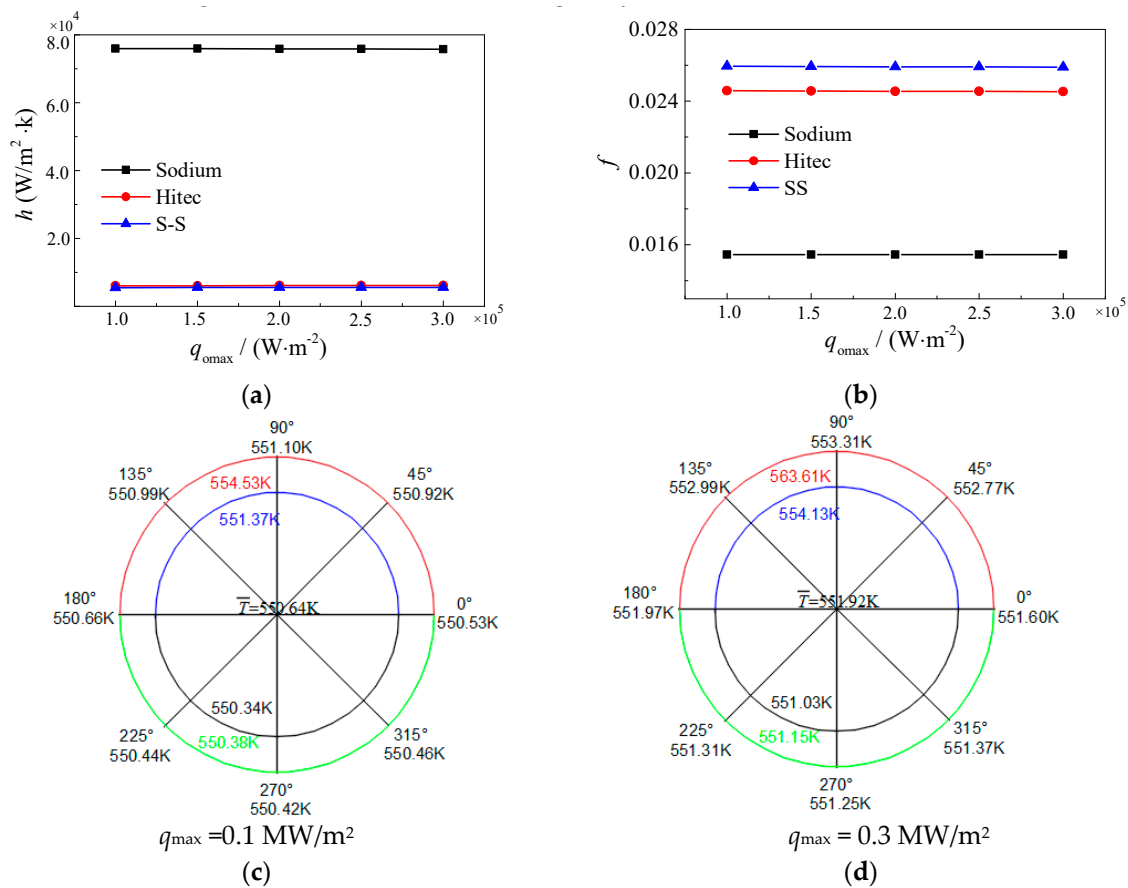


Figure 12. Effects of q_{0max} : (a) q_{0max} - h , (b) q_{0max} - f , (c,d) q_{0max} - T .

As shown in Figure 12c,d, when the maximum heat flux changed from 0.1 to 0.3 MW/m², the temperature of the outer wall increased from 554.53 °K to 563.61 °K while the average temperature of the circumferential increased by about 2 °K. At the same time, the temperature difference between the inner and outer walls is smaller than 4 °K in both cases. As a result, the thermal stress acting on the heat-transfer tubes is greatly reduced.

5. Conclusions

The heat-transfer characteristic of liquid sodium is compared with solar salt and Hitec in a heat-transfer tube for the SPT system. The calculations present the effects of operational parameters (Q_m , T_{in} , $q_{o\max}$) on the thermal and thermo-hydraulic performance of three mediums under a nonuniform heat flux. The following conclusions are obtained:

(a) The tube wall temperature difference of sodium is 20 °K, which is 4 °K lower than other the two mediums when the Re is 25,000, and the inlet temperature is 550 °K. In either NHF model or UHF model, the temperature distribution of Sodium is more uniform and higher than S-S and Hitec, and the highest temperature on the hot spot is 4 °K lower than S-S or Hitec.

(b) Among these factors (Q_m , T_{in} , $q_{o\max}$), the change of Q_m has an essential influence on the heat-transfer coefficient of HTFs. However, even in high turbulence, the thermal conductivity of Sodium still plays a crucial role. Meanwhile, the change of $q_{o\max}$ does not affect the average heat-transfer performance of the heat-transfer medium, but it has a significant influence on the temperature of the tube wall. Loading excessively high heat flux on the collector tube may cause many security issues in SPT system.

(c) Under the same boundary conditions, the heat-transfer performance of Sodium is one order of magnitude higher than that of S-S and Hitec at low temperature (550 °K~700 °K), and it is twice than the two kinds of molten salts at high temperature (700 °K +).

Author Contributions: Conceptualization, Y.H.; Data curation, J.L.; Formal analysis, J.L.; Funding acquisition, Y.H.; Investigation, J.L.; Methodology, Y.H. and X.L.; Validation, J.L.; Writing—original draft, J.L.; Writing—review & editing, J.L., Y.H. and X.L.

Funding: This work was funded by the National Natural Science Foundation of China (grant number 50876090).

Conflicts of Interest: The authors declare no conflict of interest.

References

1. Sargent and Lundy LLC Consulting Group. *Assessment of Parabolic Trough and Power Tower Solar Technology Cost and Performance Forecasts*; Report No. NREL/SR-550-34440; NREL: Golden, CO, USA, 2003. [\[CrossRef\]](#)
2. García-Barberena, J.; Monreal, A.; Mutuberria, A.; Sánchez, M. Towards cost-competitive solar towers—Energy cost reductions based on decoupled solar combined cycles (DSCC). *Energy Procedia* **2014**, *49*, 1350–1360. [\[CrossRef\]](#)
3. Hinkley, J.; Curtin, B.; Hayward, J.; Wonhas, A.; Boyd, R.; Grima, C.; Tadros, A.; Hall, R.; Naicker, K.; Mikhail, A. *Concentrating Solar Power—Drivers and Opportunities for Cost-Competitive Electricity*; Report No. EP111647; CSIRO: Canberra, Australia, 2011. [\[CrossRef\]](#)
4. Roldán, M.I.; Monterreal, R. Heat flux and temperature prediction on a volumetric receiver installed in a solar furnace. *Appl. Energy* **2014**, *120*, 65–74. [\[CrossRef\]](#)
5. Chang, C.; Li, X.; Zhang, Q.Q. Experimental and Numerical Study of the Heat Transfer Characteristics in Solar Thermal Absorber Tubes with Circumferentially Non-uniform Heat Flux. *Energy Procedia* **2014**, *49*, 305–313. [\[CrossRef\]](#)
6. Romero, M.; González-Aguilar, J. Next generation of liquid metal and other high-performance receiver designs for concentrating solar thermal (CST) central tower systems. *Adv. Conc. Sol. Therm. Res. Technol.* **2017**, 129–154. [\[CrossRef\]](#)
7. Siegel, N.P.; Bradshaw, R.W.; Cordaro, J.B.; Kruiuzenga, A.M. Thermophysical property measurement of nitrate salt heat transfer fluids. In Proceedings of the ASME 2011 5th International Conference on Energy Sustainability, Washington, DC, USA, 7–10 August 2011; pp. 439–446. [\[CrossRef\]](#)
8. Pacio, J.; Singer, C.; Wetzels, T.; Uhlig, R. Thermodynamic evaluation of liquid metals as heat transfer fluids in concentrated solar power plants. *Appl. Therm. Eng.* **2013**, *60*, 295–302. [\[CrossRef\]](#)
9. Kearney, D.; Herrmann, U.; Nava, P.; Kelly, B.; Mahoney, R.; Pacheco, J.; Cable, R.; Potrovitza, N.; Blake, D.; Price, H. Assessment of a molten salt heat transfer fluid in a parabolic trough solar field. *J. Sol. Energy Eng.* **2003**, *125*, 170–176. [\[CrossRef\]](#)

10. Thomas, W.; Julio, P.; Luca, M.; Alfons, W.; Annette, H.; Wolfgang, H.; Carsten, S.; Georg, M.; Jürgen, K.; Robert, S.; et al. Liquid metal technology for concentrated solar power systems: Contributions by the German research program. *AIMS Energy* **2014**, *2*, 89–98. [[CrossRef](#)]
11. Guidez, J.; Martin, L.; Chetal, S.; Chellapandi, P.; Raj, B. Lessons learned from sodium-cooled fast reactor operation and their ramifications for future reactors with respect to enhanced safety and reliability. *Nucl. Technol.* **2008**, *164*, 207–220. [[CrossRef](#)]
12. Singer, C.; Buck, R.; Pitz-Paal, R.; Müller-Steinhagen, H. Assessment of solar power tower driven ultrasupercritical steam cycles applying tubular central receivers with varied heat transfer media. *J. Sol. Energy Eng.* **2010**, *132*, 41010. [[CrossRef](#)]
13. Hering, W.; Stieglitz, R.; Wetzels, T. Application of liquid metals for solar energy systems. EPJ Web of Conferences. *EDP Sci.* **2012**, *33*, 03003. [[CrossRef](#)]
14. Bienert, W.B. The heat pipe and its application to solar receivers. *Electr. Power Syst. Res.* **1980**, *3*, 111–123. [[CrossRef](#)]
15. Boerema, N.; Morrison, G.; Taylor, R.; Rosengarten, G. Liquid sodium versus Hitec as a heat transfer fluid in solar thermal central receiver systems. *Sol. Energy* **2012**, *86*, 2293–2305. [[CrossRef](#)]
16. Kotzé, J.P.; von Backström, T.W.; Erens, P.J. NaK as a primary heat transfer fluid in thermal solar power installations. In Proceedings of the SolarPACES 2012 International Conference, Durban, South Africa, 27–29 March 2014.
17. Amy, C.; Budenstein, D.; Bagepalli, M.; England, D.; Deangelis, F.; Wilk, G.; Jarrett, C.; Kelsall, C.; Hirsche, J.; Wen, H.; et al. Pumping liquid metal at high temperatures up to 1,673 kelvin. *Nature* **2017**, *550*, 199–203. [[CrossRef](#)] [[PubMed](#)]
18. DeAngelis, F.; Seyf, H.R.; Berman, R.; Schmidt, G.; Moore, D.; Henry, A. Design of a high temperature (1350 °C) solar receiver based on a liquid metal heat transfer fluid: Sensitivity analysis. *Sol. Energy* **2018**, *164*, 200–209. [[CrossRef](#)]
19. Pacio, J.; Wetzels, T. Assessment of liquid metal technology status and research paths for their use as efficient heat transfer fluids in solar central receiver systems. *Sol. Energy* **2013**, *93*, 11–22. [[CrossRef](#)]
20. Pacio, J.; Fritsch, A.; Singer, C.; Uhlig, R. Liquid metals as efficient coolants for high-intensity point-focus receivers: Implications to the design and performance of next-generation CSP systems. *Energy Procedia* **2014**, *49*, 647–655. [[CrossRef](#)]
21. Matsubara, K.; Sakurai, A.; Miura, T.; Kawabata, T. Spanwise heat transport in turbulent channel flow with Prandtl numbers ranging from 0.025 to 5.0. *J. Heat Transf.* **2012**, *134*, 041701. [[CrossRef](#)]
22. Flores, O.; Marugán-Cruz, C.; Santana, D.; Garcia-Villalba, M. Thermal stresses analysis of a circular tube in a central receiver. *Int. Conf. Sol. PACES* **2014**, *49*, 354–362. [[CrossRef](#)]
23. Rodríguez-Sánchez, M.; Venegas-Bernal, M.; Marugán-Cruz, C.; Santana, D. Thermal, mechanical and hydrodynamic analysis to optimize the design of molten salt central receivers of solar tower power plants. In Proceedings of the International Conference on Renewable Energies and Power Quality (ICREPO'13), Bilbao, Spain, 20–22 March 2013; pp. 128–133. [[CrossRef](#)]
24. Irfan, M.A.; Chapman, W. Thermal stresses in radiant tubes due to axial, circumferential and radial temperature distributions. *Appl. Therm. Eng.* **2009**, *29*, 1913–1920. [[CrossRef](#)]
25. Fritsch, A.; Uhlig, R.; Marocco, L.; Frantz, C.; Flesch, R.; Hoffschmidt, B. A comparison between transient CFD and FEM simulations of solar central receiver tubes using molten salt and liquid metals. *Sol. Energy* **2017**, *155*, 259–266. [[CrossRef](#)]
26. Flesch, J.; Niedermeier, K.; Fritsch, A.; Musaeva, D.; Marocco, L.; Uhlig, R.; Baake, E.; Buck, R.; Wetzels, T. Liquid metals for solar power systems. *IOP Conf. Ser. Mater. Sci. Eng.* **2017**, *228*, 012012. [[CrossRef](#)]
27. Gartshore, I.; Salcudean, M.; Hassan, I. Film cooling injection hole geometry: Hole shape comparison for compound cooling orientation. *AIAA J.* **2015**, *39*, 1493–1499. [[CrossRef](#)]
28. Rodríguez-Sánchez, M.R.; Soria-Verdugo, A.; Almendros-Ibáñez, J.A.; Acosta-Ibáñez, A.; Santana, D. Thermal design guidelines of solar power towers. *Appl. Therm. Eng.* **2014**, *63*, 428–438. [[CrossRef](#)]
29. Patankar, S. *Numerical Heat Transfer and Fluid Flow*; Hemisphere Publishing: Washington, DC, USA, 1980.
30. Mikityuk, K. Heat transfer to liquid metal: Review of data and correlations for tube bundles. *Nucl. Eng. Des.* **2009**, *239*, 680–687. [[CrossRef](#)]
31. Minkowycz, W.J.; Sparrow, E.M.; Murthy, J.Y. *Handbook of Numerical Heat Transfer*, 2nd ed.; John Wiley & Sons: New York, NY, USA, 2000.

32. Wu, M.; Li, M.; Xu, C.; He, Y.L.; Tao, W.Q. The impact of concrete structure on the thermal performance of the dual-media thermocline thermal storage tank using concrete as the solid medium. *Appl. Energy* **2014**, *113*, 1363–1371. [[CrossRef](#)]
33. He, Y.L.; Tao, W.Q. Convective heat transfer enhancement: Mechanisms, techniques, and performance evaluation. *Adv. Heat Transf.* **2014**, *46*, 87–186. [[CrossRef](#)]
34. Gnielinski, V. New equations for heat and mass transfer in turbulent pipe and channel flow. *Int. Chem. Eng.* **1976**, *16*, 8–16.
35. Zavoico, A.B. *Solar Power Tower Design Basis Document, Revision 0*; Report of Sandia National Laboratories: San Francisco, CA, USA, 2001. [[CrossRef](#)]
36. Foust, O.J. *Sodium-NaK Engineering Handbook*; Gordon and Breach Science Publishers: New York, NY, USA, 1972; pp. 32–38.
37. VDI-Gesellschaft Verfahrenstechnik und Chemieingenieurwesen (GVC). *VDI Heat Atlas*, 2nd. ed.; Springer: Berlin, Germany, 2010.
38. Vant-Hull, L.L. The role of “allowable flux density” in the design and operation of molten-salt solar central receivers. *J. Sol. Energy Eng.* **2002**, *124*, 165–169. [[CrossRef](#)]
39. Liao, Z.; Li, X.; Xu, C.; Chang, C.; Wang, Z. Allowable flux density on a solar central receiver. *Renew. Energ.* **2014**, *62*, 747–753. [[CrossRef](#)]



© 2019 by the authors. Licensee MDPI, Basel, Switzerland. This article is an open access article distributed under the terms and conditions of the Creative Commons Attribution (CC BY) license (<http://creativecommons.org/licenses/by/4.0/>).